Effect of Mo and V on the Hydrothermal Crystallization of Hematite from Ferrihydrite: An *in Situ* Energy Dispersive X-ray Diffraction and X-ray Absorption Spectroscopy Study

Loredana Brinza,*[†,⊥] Hong P. Vu,[‡,⊥] Samuel Shaw,[§,⊥] J. Fred W. Mosselmans,[∥] and Liane G. Benning*[⊥,#]

[†]Department of Interdisciplinary Research, "Alexandru Ioan Cuza" University of Iasi, Lascar Catargi Str., No 54, 700107 Iasi, Romania
[‡]School of Earth Sciences, Faculty of Science, University of Melbourne, Victoria 3010 Australia
[§]School of Earth, Atmospheric and Environmental Sciences, University of Manchester, Manchester M13 9PL, United Kingdom
[∥]Diamond Light Source, Harwell Science and Innovation Campus, Didcot, Oxfordshire OX11 0DE, United Kingdom
[⊥]Earth Surface Science Institute, School of Earth and Environment, University of Leeds, Leeds LS2 9JT, United Kingdom
[#]GFZ German Research Centre for Geosciences, Telegrafenberg, Potsdam 14473, Germany

Ⓢ *Supporting Information*

ABSTRACT: In this study we used *in situ* synchrotron-based energy dispersive X-ray diffraction (EDXRD) to follow the transformation of ferrihydrite to hematite at pH $\sim$ 8 and ionic strength between 0.1 and 0.7. In addition, the effects of coprecipitated molybdenum (Mo) and vanadium (V) on the transformation were evaluated both through EDXRD and X-ray absorption spectroscopy (XAS). The transformation end product in all experiments was hematite with small amounts of goethite as an intermediate phase. XAS results revealed that Mo and V were initially adsorbed and coprecipitated onto/with ferrihydrite as molybdate and vanadate ions, respectively. After the ferrihydrite transformed to hematite these metals were sequestered into the hematite structure. The kinetic results showed that the presence of Mo and V in the ferrihydrite structure had little to no effect on the kinetics of the ferrihydrite transformation. The transformation however occurred $\sim$30% faster at higher ionic strength.
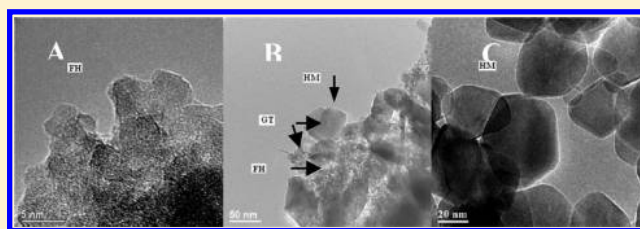
INTRODUCTION

Iron (oxyhydr)oxide mineral phases (e.g., ferrihydrite, FH, $Fe_5O_3(OH)_9$; goethite, GT, α-FeOOH; hematite, HM, α-Fe_2O_3) are important components of the iron cycle in many environmental systems, including soils and marine sediments.[1] Furthermore, owing to their high surface areas[1] (up to 700 m² g⁻¹), iron (oxyhydr)oxide phases have a high adsorption capacity for trace elements from solution.[2,3] They also have a high capacity to take up trace elements via coprecipitation.[4,5] These properties are important in both natural and contaminated environments[6] as these phases can control the bioavailability of nutrients (i.e., phosphate[7]) and contaminants (e.g., arsenic and lead) in soils,[8−12] sediments, water columns, or wastewater treatment plants.[1] Ferrihydrite is also an important oxidation product in hydrothermal plumes of deep sea hydrothermal vents when acidic, high temperature (350−400 °C) fluids containing elevated iron concentration come into contact with seawater (pH = 8.3; ionic strength of $\sim$0.7, T = 2−4 °C).[13] This process results in hydrothermal vents being a significant source of particulate iron to the global ocean ($\sim$50 Gg yr⁻¹).[14] Iron oxihydroxide particulate phases in hydro-thermal plumes can scavenge a wide variety of trace elements from seawater (e.g., phosphorus,[15] vanadium,[16,17] arsenic,[18]

molybdenum,[19,20] lead, and rare-earth elements[21]). In addition, during the crystallization of ferrihydrite, any coprecipitated or adsorbed metals can be either released back into solution or sequestered by the newly formed crystalline phases.[11,16,22] Currently, relatively little is known about what controls these processes, and it is, therefore, crucial that we understand the availability and fate of trace metals during the formation and crystallization of iron (oxyhydr)oxide phases.

Molybdenum (Mo) and vanadium (V) are important elements for marine and surface phyto- and zoo-plankton. For example, Mo catalyzes the electron transfer reaction in nitrogen fixation[23,24] and nitrate reduction,[25] and V is an essential cofactor for enzymatic processes involved in plant growth.[26] In contrast, at high concentrations, both Mo and V, in particular V(V), can become toxic to plants, animals, and humans. For examples, Mo in concentrations of up to 30 mg L⁻¹ in the diet of sheep inhibits copper uptake in the gastrointestinal tract leading to molybdenosis.[27] V becomes toxic in marine system when its concentration is above 100 μg

L^{-1} (6-day LC50 for fish is 0.5−22 mg L^{-1}), whereas V in soils at concentrations of 10 mg kg^{-1} or more is toxic for terrestrial plants.[28] For humans long-term exposure to excess Mo leads to loss of appetite, diarrhea, anemia, and slow growth,[27] whereas V exposure reduces the number of red blood cells, increases blood pressure, and even leads to neurological effects.[29] Furthermore, marine studies have shown that Mo isotopic fractionation in ferromanganese crusts and sediments may be used as a potential proxy for global paleo-ocean redox conditions.[30] In addition, V/Fe ratios in hydrothermal fractions of marine sediments have been found to be similar to V/Fe ratios in hydrothermal plume particles. These in turn have been found to correlate with dissolved phosphate in seawater, and thus could be useful as a tracer of dissolved phosphate in past oceans.[31]

Ferrihydrite is a metastable and poorly ordered iron oxyhydroxide phase that is often the first phase to form from solution when dissolved ferric iron hydrolyzes.[1] This nanoparticulate phase is thermodynamically unstable with respect to crystalline iron (oxyhydr)oxide phases (e.g., goethite and hematite) under environmental conditions. The kinetics, rate and products of ferrihydrite crystallization are influenced by a number of factors including pH,[32] temperature,[33] solid/solution ratio, and presence of different anions (nitrate, chloride, sulfate, and phosphate),[33,34] or cations (e.g., cadmium, lead,[11,35] and ferrous iron[36]) which can either inhibit or catalyze the crystallization reactions. pH is one of the primary parameters which influences the kinetics and mechanisms of iron oxyhydroxides' transformation, as it controls the surface properties of the particles (e.g., surface charge) and speciation/concentration of ions in the reacting solutions. Extensive studies have been carried out on ferrihydrite crystallization as a function of pH and temperature (room temperature to >200 °C), at low ionic strength conditions.[37−40] Overall, the transformation of ferrihydrite to hematite/goethite is controlled by the pH dependent solubility of ferric iron.[41] Hematite is the dominant end product at near neutral pH where iron solubility is lowest, where the transformation occurs via the aggregation of ferrihydrite particles followed by a dehydration/recrystallization process. In contrast, at both acidic and alkaline pH (i.e., 2−5 and 10−14), ferric iron solubility is higher and goethite is the dominant end product forming via a dissolution and reprecipitation mechanism. These conclusions have been drawn from, for example, studies by Schwertmann and Murad[24] and Schwertmann et al.[32] who showed that, at pH values of 7−8, close to the point of zero charge (PZC) of ferrihydrite, hematite is the favored end product. At low temperatures and alkaline pH (>10−11) goethite is the favored end product,[32,37,40] although at high temperature goethite is an intermediate phase and hematite is the main final end product.[33,42,43] Ionic strength is another parameter which has a complex influence on solubility[44] and consequently mineral nucleation and growth.[1,45,46] Due to the complexity of the various mineral formation mechanisms and the related effects of various chemical parameters (e.g., pH, solution saturation,[47] presence of other competitive ions, size of seeding crystal[45]) on each specific process, these trends cannot be generalized, and thus, there is a need for them to be studied individually.

There are a limited number of studies of Mo or V uptake via adsorption onto ferrihydrite[19,48−50] and its fate during crystallization. We are also not aware of any studies which investigated the coprecipitation of Mo or V with ferrihydrite and their effect and fate upon its crystallization at near neutral

pH. Thus, this research focused on (i) evaluating the partitioning of Mo and V, which have been adsorbed onto or coprecipitated with ferrihydrite, during transformation to hematite; (ii) assessing local bonding environments of Mo and V when adsorbed and coprecipitated with ferrihydrite (initial material), and hematite (the final end product) using X-ray absorption spectroscopy (XAS); and (iii) determining the effect of high temperature, high ionic strength, and the presence of Mo and V on the kinetics of ferrihydrite crystallization to hematite at pH 8 using *in situ* synchrotron-based energy dispersive X-ray diffraction (EDXRD).

■ METHODOLOGY

Pure Ferrihydrite Synthesis: Starting Materials. Pure 2-line ferrihydrite was synthesized following the method of Cornell and Schwertmann[51] by slow titration of a 0.127 M Fe $(NO_3)_3 \cdot 9H_2O$ solution with a 1.0 M sodium hydroxide solution. The obtained slurry was washed 5 times with distilled water in consecutive dispersion and centrifugation cycles, until the concentration of total dissolved solids in the slurry was less than 20 mg L^{-1} (measured using a Hanna DiST1 TDS meter). The density of the washed ferrihydrite slurry was determined from the weight ratio of triplicate subsamples measured before and after drying at 50 °C for 16 h. The slurry was stored in a fridge (4 °C) for a maximum of 1 week prior to use in the metal adsorption and transformation experiments.

Ferrihydrite Transformation: Microscopy and XRD. *Ex situ* test batch experiments were carried out at 160 and 200 °C using a pure FH slurry [14 g dry FH L^{-1}, IS (ionic strength) of 0.01 (to mimic fresh water conditions) and 0.7 (to mimic seawater conditions) at near neutral pH (initial pH was 8)], without *in situ* EDXRD data collection. The ionic strength was adjusted using a 1 M NaCl solution. The experiments were conducted in Teflon-lined Parr steel hydrothermal reactors (total volume of 20 mL). Experiments carried out at the Synchrotron Radiation Source (SRS, $T \leq 200$ °C were controlled by a heating block fitted with four heating cartridges and a thermocouple to ensure a constant temperature during the experiments) were up to 8 h, and experiments carried out at the University of Leeds (in the oven, at 160 °C) were up to 24 h.

At select time points during the experiments, the reactions were quenched, and the solids were separated from the supernatants, washed by MQ water, and analyzed by high resolution field emission gun transmission electron microscopy (HR-FEG-TEM, Philips/FEICM200) operated at 197 keV and fitted with an energy dispersive X-ray spectrometer (EDS). The initial, intermediary, and end product solids were analyzed using a conventional X-ray diffractometer (Philips PW 1730/10, Cu Kα, λ = 1.54 Å). Changes in the pH were monitored at the beginning and the end of the experiments. Ferrihydrite dissolution was quantified by measuring the dissolved iron concentration (using the Ferozzine method[52]) in the supernatant at the end of the experiments.

Partitioning of Mo/V During Ferrihydrite Transformation. *i. Adsorption and Coprecipitation Experiments.* Mo and V adsorption experiments were carried out in 500 mL batch reactors at pH 7. The concentration of FH was 2 g L^{-1}, and the initial concentration of Mo/V was 1000 μM. The pH was checked throughout the adsorption experiments and adjusted to a constant value with 0.01 M NaOH or 0.01 M HCl when needed. The adsorption experiments were run for 24 h as sacrificial replicates to ensure that there was always enough solid material for evaluating the ferrihydrite transformation products both after adsorption and at the end of the transformation experiment, including desorption post-transformation. The amount of Mo and V adsorbed onto ferrihydrite was calculated from the mass balance, as the difference between the initial added and post adsorption metal values measured in the supernatant by inductively coupled plasma optical emission spectrometry (PerkinElmer Optima ICP-OES).

Ferrihydrite coprecipitated with Mo (Mo-FH) and V (V-FH) was prepared by synthesizing batches of ca. 10 g of FH in ca. 800 mL of

solution in the presence of 1000 μM Mo/V. Mo solution was made from $Na_2MoO_4 \cdot 2H_2O$, VWR BDH AnalaR, 99.5% (added to the basic solution of synthesis), and vanadium from Na_3VO_4, Sigma-Aldrich, 99.98% (added to the ferric solution prior to mixing). The Mo and V content in the resulting ferrihydrite samples were determined by mass balance of Mo and V initially added and finally measured in the coprecipitated slurry supernatant (after filtration through 0.2 μm filters) measured via ICP-OES. For each coprecipitated ferrihydrite batch the density was determined by dry weight (in triplicate, at 50 °C, for 16 h). After washing by MQ water the resulting slurries had densities of 0.041 g FH g^{-1} slurry (for Mo-FH) and 0.042 g FH g^{-1} slurry (for V-FH). These slurries were stored in the dark, at 4 °C and pH 7 for maximum of 1 week prior to initiating the off-line transformation experiments.

ii. Off-Line Transformation Experiments. The freshly made Mo/V-adsorbed and coprecipitated ferrihydrite slurries were transformed to hematite at 150 °C and pH 8 in Teflon-lined Parr steel hydrothermal reactors (in a Binder FP series oven) for ~2 days. For transformation experiments 0.25 g FH was added to 10 mL of solution in Teflon-lined Parr steel hydrothermal reactors, leading to a ferrihydrite concentration in transformation experiments of 25 g dry FH L^{-1}. The transformed samples were centrifuged at 8000 rpm for 15 min to separate the solid from the supernatant, and the transformation end product solids were analyzed by XRD while the supernatant solutions were filtered through 0.2 μm acetate cellulose syringe filter and acidified for the analysis of Mo and V by ICP-OES.

iii. Desorption Experiments. A desorption step was used to quantify the amount of Mo or V associated with the hematite surface after the transformation.[53] Sacrificial replicates of the post-transformation samples were centrifuged, and the separated solids were equilibrated under constant stirring conditions with a 2 M NH$_4$OH solution (0.25 g solids/10 mL, pH > 11) for 30 min (a short time to avoid/minimize iron oxyhydroxides dissolution, but sufficient for surface desorption to take place). The supernatant was collected by centrifugation, filtered, and analyzed for Mo and V concentrations by ICP-OES. The remaining hematite was digested in 6 M HCl, and the resulting solution was analyzed by ICP-OES to quantify Mo and V contents within the mineral particles (structure).

Bonding Environment of Mo and V Associated with Coprecipitated Ferrihydrite and Hematite: XAS Study. Synchrotron-based X-ray absorption spectroscopy (XAS) was used to investigate the bonding environment of Mo and V associated with (i) ferrihydrite (Mo/V ads FH or Mo/V copp FH); (ii) hematite as end product from ferrihydrite transformation (Mo/V ads FH -tr or Mo/V copp FH- tr); and (iii) the hematite after the desorption step (Mo/V ads FH-tr-des or Mo/V copp FH-tr-des). The adsorption, coprecipitation, off-line transformation, and desorption processes were carried out as described above at temperatures between 160 and 200 °C and at a pH of 7. For the Mo system two extra sets of experiments were considered: (a) adsorption and coprecipitation experiments with different initial Mo concentrations in solutions [1, 10, 100, 1000 μM (and 1 g FH L^{-1} at pH 7 and T = 30 °C)] to evaluate whether Mo forms specific Mo phases/clusters/polymers, and (b) adsorbed and coprecipitated samples with 1000 μM Mo transformed at pH 7 and at pH 8.5 at the same temperature (T = 150 °C) to assess whether the initial transformation pH influenced the bonding environment of Mo in the hematite end product. In the results XAS samples will be named using initial Mo/V concentration used in experiment (i.e., Ads/Copp 1/10/100/1000 μM Mo/V).

XAS measurements were carried out at the Synchrotron Radiation Source (SRS), at the Daresbury Laboratory at station 16.5[54] for Mo, and at the Diamond Light Source (DLS), at the I18[55] microfocus spectroscopy beamline for V. Station 16.5 was equipped with a water-cooled Si (220) double crystal monochromator (DCM) and a 30 element monolithic Ge fluorescence solid state detector. Harmonic rejection was achieved by use of a plane mirror. In contrast station I18 is equipped with a cryocooled (Si 111) DCM, and a 9 element Ge detector; harmonic rejection was achieved using a Si stripe on one of the microfocusing mirrors, which was defocused for this experiment. Data was collected from the Mo ferrihydrite samples using a liquid

nitrogen cooled cryostat at 80 K, whereas data was collected from the V samples at room temperature. Two regimes were considered from the XAS spectra: X-ray absorption near edge structure (XANES) and extended X-ray fine structure (EXAFS). The interpretation of the XANES gives information about the oxidation state and coordination chemistry of the absorbing atom, while EXAFS is used to determine bond and interatomic distances, coordination number, and species of the neighbors of the absorbing atom. Samples from the coprecipitation and adsorption experiments containing Mo/V in the initial system from 1 to 1000 μM were examined in fluorescence mode, while the standards were run in transmission mode. Synthetic and natural standards (Na_2MoO_4, K_2MoO_4, and MoO_3 for molybdenum and Na_3VO_4 and V_2O_5 for vanadium) were analyzed. Where necessary, the standards were diluted appropriately with an inert diluting salt, boron nitride. All standards were analyzed by conventional XRD to confirm their identity and purity.

Data normalization and linear combination analysis were done using the Athena software. EXAFS data fitting, with coordination numbers as integer numbers, was carried out using the Artemis software using Feff 6. Athena and Artemis are both part of the Demeter package.[56] The goodness of EXAFS data fitting is given by R factor, which represents the absolute misfit between the theory and the data.

Transformation Kinetics: Energy Dispersive X-ray Diffraction. *i. On-Line, in Situ, Transformation Experiments.* Time-resolved EDXRD measurements were performed at SRS Daresbury Laboratory on station 16.4. The use of EDXRD allows for monitoring of changes in diffraction intensities during *in situ* and time-resolved crystallization experiments in solution. For this, a polychromatic X-ray beam was directed toward the sample (15 mL of a 50 g L^{-1} ferrihydrite slurry at pH 8) contained in a Teflon-lined steel hydrothermal reactor. For the pure FH, Mo-FH, and V-FH systems, experiments were carried out at an ionic strength (IS) of 0.7 (adjusted with 1 M NaCl) and at temperatures between 130 and 240 °C. For the Mo-FH system an experiment was also carried out at IS = 0.1 at 160 °C. The reaction cells were isothermally equilibrated at a constant temperature and the contents stirred via a magnetic stirring incorporated within the heater housing of the reaction system. The diffracted beam was detected by three solid detectors. Further details about similar *in situ* experiments, the station setup, and data acquisition can be found in Shaw et al.[33] and Davidson et al.[42] Experiments were conducted for between 10 and 160 min, with diffraction patterns recorded every minute. Initial and final pH values (measured with a ORION 710A pH meter) as well as iron concentrations (analyzed by Ferrozine[52]) in the filtered final solutions were also measured. Upon completion of each experiment the solid end products were separated by filtration, washed, and analyzed with a conventional XRD to check for possible minor phases not detectable by EDXRD.[57] The progress of the crystallization reaction was evaluated through the change in the normalized area of the Bragg peaks of hematite (and goethite) calculated using XFIT[58] and expressed as

$$\alpha = (A_t - A_{min})/(A_{max} - A_{min}) \qquad (1)$$

where α is the degree of reaction, A_t is the peak area at time t, A_{min} is the minimum (time at which the Bragg peak first appeared), and A_{max} was the maximum peak area. The (110) peaks for hematite and goethite were chosen as they are distinct and high intensity peaks that clearly differentiate hematite from goethite in mixed phase samples.[11,59]

ii. Kinetic Evaluation and Activation Energies. The growth of (110) Bragg peaks from the EDXRD data was fitted with the Johnson–Mehl–Avrami–Kolmogorov (JMAK) kinetic model[60−62] to obtain kinetic parameters of the ferrihydrite transformation to hematite

$$\alpha = 1 - e^{-k(t-t_0)^m} \qquad (2)$$

where k is the rate constant for the reaction (s^{-1}), t is time (s), t_0 is the induction time (s), and m is a constant that depends on the reaction mechanism and the dimensionality of growth.[63] The fits were performed in Origin 8.[64] Indeed, several other kinetic models for phase transformations are available in the literature[65,66] and were
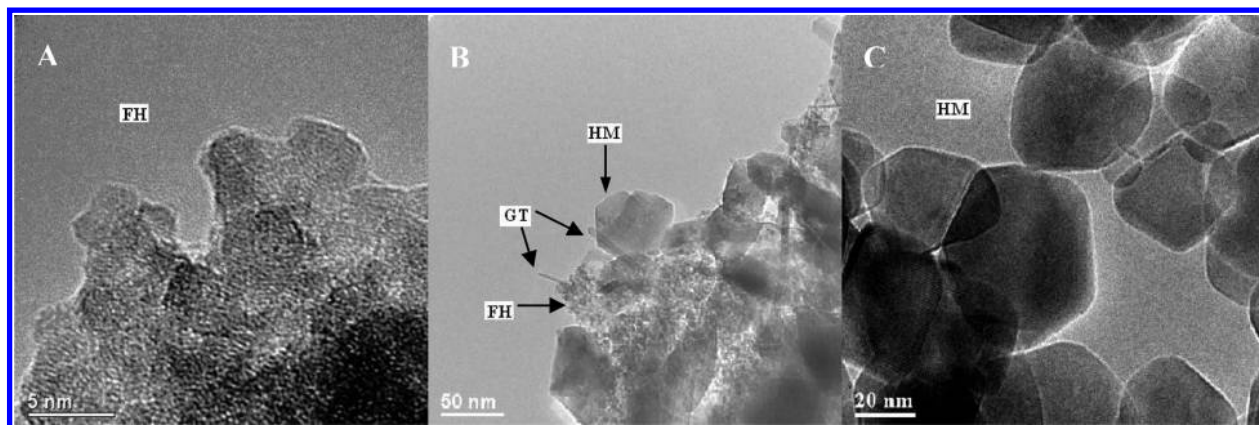
Figure 1. Representative FEG-TEM images of (A) the starting material, ferrihydrite (FH); (B) intermediate phases consisting of hematite, ferrihydrite, and minor goethite (GT) as intermediate; and (C) end product, hematite (HM) from the *ex situ*, pure ferrihydrite transformation experiment at T = 160 °C.

considered. However, the JMAK model was selected due to its simplicity and popularity, and because it describes our data best (see below).

The apparent activation energies of crystallization of the end products were calculated from the Arrhenius equation:

$$k = Ae^{-E_a/RT} \tag{3}$$

where k is the rate constant, A is the frequency or pre-exponential factor, E_a is the activation energy (kJ mol^{-1}), R is the gas constant (8.314 J mol^{-1} K^{-1}), and T is the absolute temperature in K. For comparison, the "time to a given fraction method"[67] was also used to determine the activation energy of crystallization. This approach relies solely on the time to a given fraction of transformation (t^*) as a function of temperature and can be expressed as

$$\ln t^*_\alpha = \text{const} - \ln A + (E_a/R)(1/T) \tag{4}$$

where the t^* is the time of the given fractionation which was chosen (usually, 50% transformation), in seconds.

■ RESULTS AND DISCUSSION

Ferrihydrite Transformation to Hematite at Neutral pH. High resolution TEM images were collected from the ferrihydrite starting materials, intermediate reaction stage samples, and the reaction end products (Figure 1A−C) from the *ex situ* experiment with pure ferrihydrite reacted at 160 °C. Images of the starting material showed that ferrihydrite consisted of aggregated nanoparticles <5 nm in size, which is in agreement with previous TEM observation of 2-line ferrihydrite.[68] After a few hours, the slurry consisted of a mixture of 2-line ferrihydrite nanoparticles and hexagonal hematite plates, with minor quantities of goethite (small marked needles in Figure 1B). Finally, the end product was pure hematite (Figure 1C) consisting of hexagonal platelets of varying size.

Off-line XRD results from this transformation experiment (Figure SI 1), supported by TEM data, are in good agreement with literature studies of hematite crystallization from ferrihydrite under near neutral pH conditions.[37,40] Measurements of pH at the end of experiments showed a decrease in pH (~6) and no dissolved iron (<0.001 mg L^{-1}) in the supernatant.

Partitioning of V and Mo During and after Ferrihydrite Transformation. Table 1 summarizes the three different metal pools: solution (in supernatant solution after transformation), surface (release after desorption), and structure

Table 1. Partitioning of V and Mo Adsorbed onto and Coprecipitated with Ferrihydrite and after Ferrihydrite Transformation to Hematite (Initial pH 7, Initial Mo/V Concentration 1000 μM)

partitioning/uptake pool	adsorption		coprecipitation	
	Mo	V	Mo	V
% in solution	3.5	0.0	3.2	0.01
% on surface (i.e., adsorption)	6.4	4.1	2.7	0.0
% structurally incorporated	90.1	95.9	94.1	100

(retained in the hematite structure after desorption) for V and Mo associated with the iron (oxyhydr)oxides.

The partitioning data for the Mo coprecipitated ferrihydrite experiment revealed that only ~3% of the Mo remained in the reacting solution after the transformation and ~3% of the total Mo was bound to the surface of the hematite, with the remaining >94% structurally incorporated. Interestingly, all V that was coprecipitated with the initial ferrihydrite became incorporated into structure of the hematite end product. For the adsorption experiments the partitioning results showed that ca. 4% of Mo and 0% of V remained in the solution after the transformation, ~6% of Mo and 4% of V was bound to the surface, and 90% of Mo and 96% of V were structurally incorporated.

The majority of the Mo and V in both systems (via coprecipitation and via adsorption) became sequestered in the end product structure.

Bonding Environment of Mo and V Associated with Coprecipitated Ferrihydrite and Hematite: XAS. The Mo X-ray absorption spectra of the ferrihydrite coprecipitated and adsorbed with various Mo concentrations showed no differences indicating that Mo did not polymerize or form specific precipitates in these systems and that its bonding environment was similar over the range of concentrations used (see Figure SI 5 for EXAFS spectra as example). Thus, only samples from the highest working concentrations are discussed below.

Mo XAS. Figure 2 displays K-edge Mo X-ray absorption near-edge structure (XANES) profiles of the adsorbed (Figure 2A) and coprecipitated (Figure 2B) samples and the appropriate standards (i.e., Na$_2$MoO$_4$ and MoO$_3$).

The Mo K-edge XANES spectra for both Mo-adsorbed ferrihydrite and Mo coprecipitation ferrihydrite are alike and very similar to the spectrum of the Na$_2$MoO$_4$ standard: with
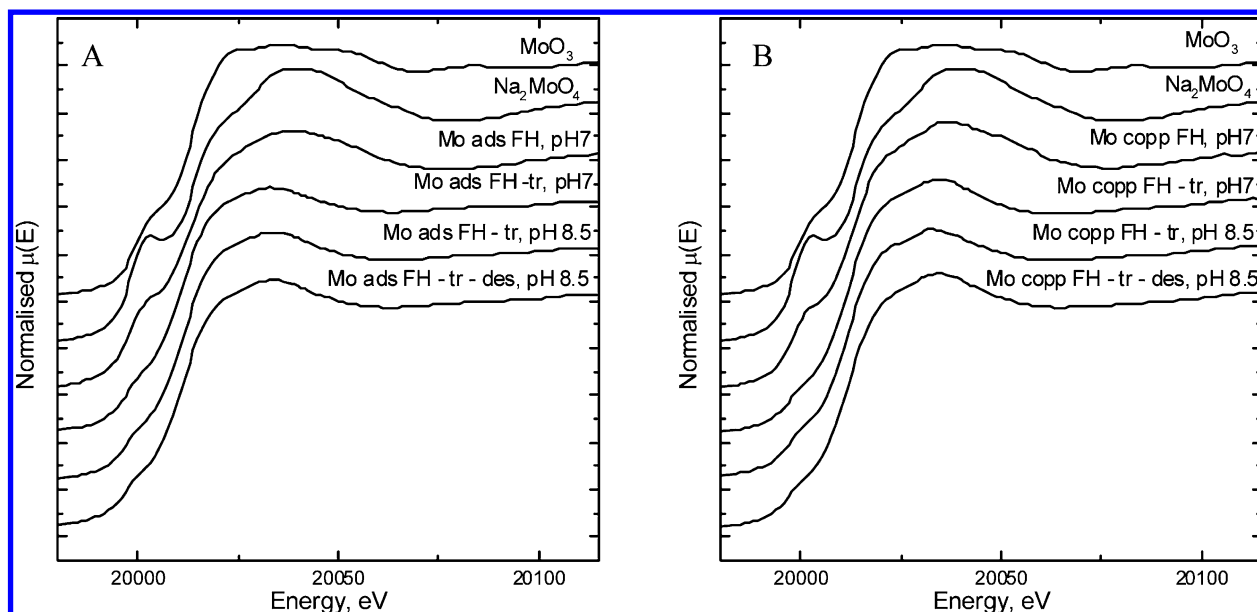
Figure 2. Mo K edge XANES spectra for (A) adsorption samples and (B) coprecipitated samples and standards.
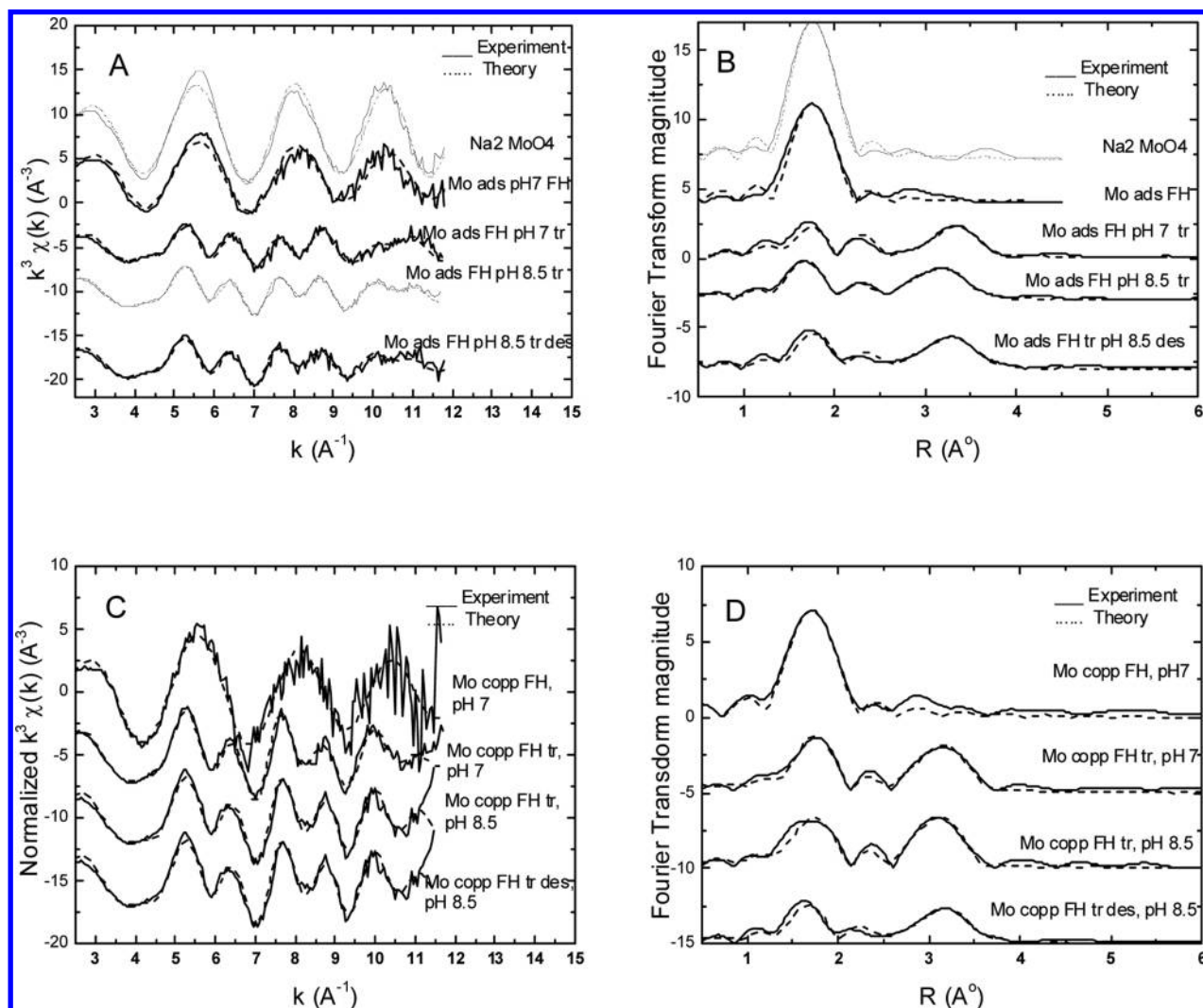

Figure 3. Summary of k^3 weighted Mo K-edge EXAFS spectra (A and C) and phase corrected Fourier transforms (B and D) for EXAFS spectra for adsorbed (A and B) and coprecipitated (C and D) samples and Na$_2$MoO$_4$ standard.

Table 2. Summary of Mo EXAFS Fit Parameters and Crystallographic Information of Appropriate Standards

| sample	path	path degeneracy	bond distance R (Å)	σ^{2e}	R-factor[f]
Na$_2$MoO$_4$	Mo–O	4	1.76 ± 0.01	0.001 ± 0.001	0.007
Na$_2$MoO$_4$[a]	Mo–O	4	1.76		
MoO$_3$[c]	Mo–O	2	1.68		
	Mo–O	2	1.92		
	Mo–O	2	2.28		
MoO$_3$[b]	Mo–O	2	1.67		
		2	1.96		
Mo ads FH, pH 7	Mo–O	4	1.76 ± 0.01	0.03 ± 0.001	0.008
Mo ads FH tr, pH 7	Mo–O	2	1.74 ± 0.07	0.004 ± 0.002	0.028
	Mo–O	3	1.97 ± 0.01	0.007 ± 0.002	
	Mo–Fe	1	2.89 ± 0.06	0.012 ± 0.011	
	Mo–Fe	3	3.08 ± 0.01	0.007 ± 0.003	
	Mo–Fe	3	3.45 ± 0.03	0.014 ± 0.005	
Mo ads FH tr, pH 8.5	Mo–O	2	1.76 ± 0.01	0.006 ± 0.002	0.010
	Mo–O	3	1.99 ± 0.02	0.011 ± 0.003	
	Mo–Fe	1	2.89 ± 0.05	0.010 ± 0.006	
	Mo–Fe	3	3.06 ± 0.02	0.007 ± 0.002	
	Mo–Fe	3	3.50 ± 0.03	0.013 ± 0.004	
Mo ads FH tr des, pH 8.5	Mo–O	2	1.76 ± 0.009	0.005 ± 0.002	0.024
	Mo–O	3	1.99 ± 0.02	0.012 ± 0.004	
	Mo–Fe	1	2.96 ± 0.08	0.013 ± 0.018	
	Mo–Fe	3	3.09 ± 0.02	0.008 ± 0.003	
	Mo–Fe	3	3.53 ± 0.04	0.018 ± 0.007	
Fe in hematite[d]	Fe–O	3	1.94		
	Fe–O	3	2.11		
	Fe–Fe	1	2.89		
	Fe–Fe	3	2.96		
	Fe–Fe	3	3.36		
Mo copp FH pH 7	Mo–O	4	1.76 ± 0.01	0.03 ± 0.002	0.012
Mo copp FH tr, pH 7	Mo–O	3	1.80 ± 0.02	0.007 ± 0.003	0.020
	Mo–O	3	2.05 ± 0.05	0.016 ± 0.005	
	Mo–Fe	1	2.98 ± 0.12	0.012 ± 0.024	
	Mo–Fe	3	3.09 ± 0.04	0.008 ± 0.005	
	Mo–Fe	3	3.48 ± 0.05	0.019 ± 0.010	
Mo copp FH tr, pH 8.5	Mo–O	3	1.79 ± 0.01	0.009 ± 0.004	0.031
	Mo–O	3	2.05 ± 0.04	0.017 ± 0.004	
	Mo–Fe	1	2.94 ± 0.08	0.013 ± 0.016	
	Mo–Fe	3	3.08 ± 0.02	0.007 ± 0.003	
	Mo–Fe	3	3.44 ± 0.11	0.029 ± 0.019	
Mo copp FH tr des, pH 8.5	Mo–O	3	1.79 ± 0.01	0.009 ± 0.004	0.031
	Mo–O	3	2.05 ± 0.04	0.017 ± 0.004	
	Mo–Fe	1	2.94 ± 0.08	0.013 ± 0.016	
	Mo–Fe	3	3.08 ± 0.02	0.007 ± 0.003	
	Mo–Fe	3	3.44 ± 0.11	0.029 ± 0.019	

[a]Na$_2$MoO$_4$ structure (ICSD 4156) after Matsumoto et al.[70] [b]MoO$_3$ structure after Radhakrishnan et al.[72] [c]MoO$_3$ structure of MoO$_3$ standard refined from XAFS data using Excurv98.[49] [d]Hematite structure (ICSD 56369) after Wolska and Schwertmann.[71] [e]σ^2 is the mean-square disorder in the distribution of interatomic distances.[56] [f]R-factor is the sum of the residual: a measure of the percentage misfit between the data and theory.[56]

pre-edge feature at 20 002 eV, adsorption edge at 20 015 eV, and the top of the white line at 20 040 eV, respectively. The XRD also confirmed that in the Mo adsorbed and coprecipitated ferrihydrite samples no other Mo mineral phases formed. The lower intensity of the pre-edge feature in samples compared with standard may indicate some structural disorder in the Mo adsorbed and coprecipitated samples. In general, Mo K-edge XANES results suggest that Mo(VI) is largely taken up into ferrihydrite as the molybdate species, and that it is tetrahedrally coordinated, both in the adsorption and coprecipitation systems. For the Mo adsorbed onto ferrihydrite samples this matches well with previous findings.[19,20,69]

The post-transformation samples have different XANES spectra compared with those of Mo ferrihydrite samples: in particular, the peak of the white line is shifted by approximately −5 eV, and the pre-edge peak (at 20 003 eV) is much less pronounced. These differences may suggest that Mo(VI) has adopted a distorted octahedral geometry (seen in MoO$_3$ standard), in the post-transformation hematite samples.

For the freshly adsorbed and coprecipitated ferrihydrite samples the Mo k^3 weighted EXAFS and Fourier transformed fitting results are in good agreement with our interpretation of the Mo K-edge XANES. The Mo k^3 weighted EXAFS plots (Figure 3A,C) show similar amplitude shapes for the freshly
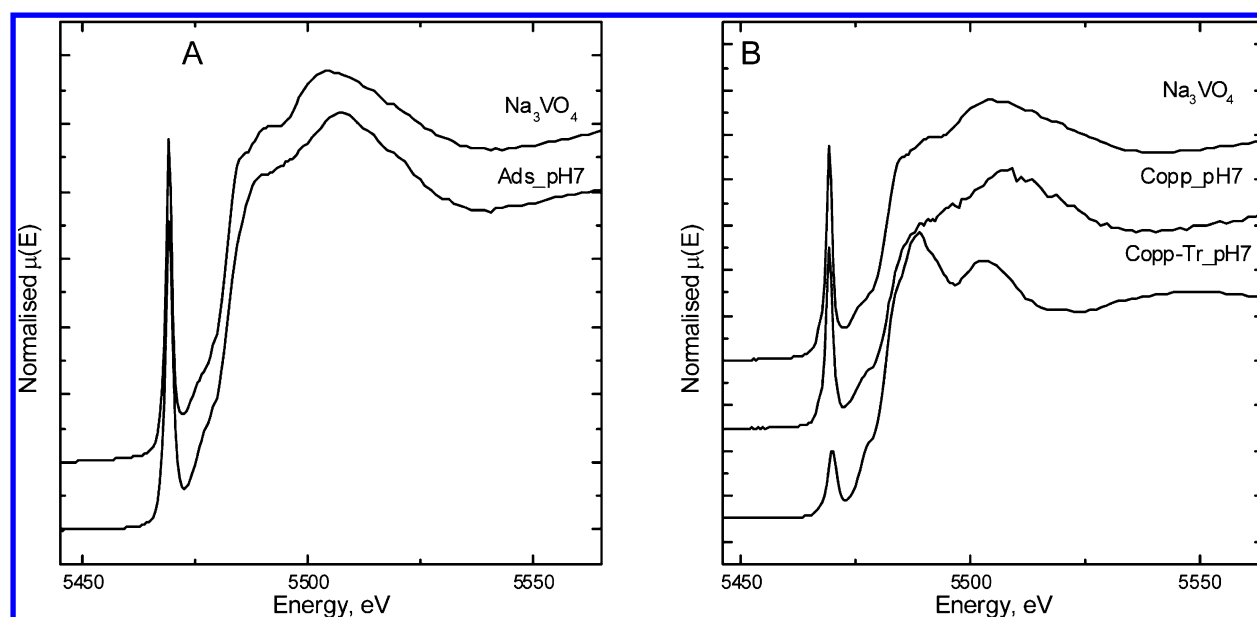
Figure 4. V K edge XANES spectra for (A) adsorption samples and (B) coprecipitated samples and Na_3VO_4 standards.

Mo adsorbed and coprecipitated ferrihydrites and Na_2MoO_4 standard, but with different intensities. Fits of the adsorbed (Figure 3A) and coprecipitated (Figure 3C) species indicate that there are four oxygen atoms situated in the first shell at a bond distance of 1.76 Å from the main Mo atom. This is indicative of tetrahedrally coordinated Mo in molybdate, which agrees with previous literature findings that reported that Mo adsorbs as an outer sphere molybdate species onto ferrihydrite surfaces[19,20,70] (Table 2). The differences in the intensities for the adsorbed and coprecipitated samples are correlated with the variations in the σ^2 factors and indicate different degrees of disorder for the molybdate species associated with the ferrihydrite structure.

As the Mo XANES suggests that Mo may be octahedrally coordinated in the transformed samples an attempt was made to fit our Mo post-transformation spectra to a model in which Mo substitutes for the octahedral iron in hematite. The results together with hematite structural data from Wolska and Schwertmann[71] are presented in Table 2. The hematite structure is formed of a succession of oxygen octahedra (with the Fe(III) ions residing inside) and empty tetrahedral interstitial sites. There are various Fe—Fe distance in the hematite structure corresponding to different octahedral linkages: 3.70 and 3.34 Å specific to double corner sharing octahedra; 2.97 Å specific to edge sharing octahedra, and 2.89 Å specific to face sharing octahedral sites. In hematite Fe has two shells of three oxygen atoms at distances of 1.94 and 2.11 Å, respectively (Table 2).

All adsorbed samples post-transformation (and desorption) fitted well to a model comprising two oxygen distances in the first coordination sphere: two oxygen atoms at 1.74−1.76 Å and three oxygen atoms at 1.97−1.99 Å. There are three Fe shells at distances ranging 2.89−2.96, 3.06−3.09, and 3.45−3.53 Å. When the coordination number (5 for the O shell) and interatomic distances (smaller) of the Mo−O/Fe shells in the Mo associated hematite samples are compared with Fe−O distances in pure hematite, the comparison suggests that Mo in our samples was mainly accommodated in octahedral sites of the hematite structure. Further, iron shells with varying

interatomic distances compared to pure hematite may indicate different substitution degrees of Mo in the hematite structure.

For the coprecipitated and transformed samples, larger interatomic distances for oxygen in the first and second shells at 1.79/80 and 2.05 Å as well as bigger iron interatomic distances at 2.94/8, 3.08/9, and 3.44/8 Å may indicate possible distortions of the Mo octahedra within the hematite structure (or a mixture of Mo occupied Fe octahedral sites in hematite). Variable σ^2 factors of the fits as well as different interatomic distance errors (i.e., slightly larger for the first and third iron shells) among the coprecipitated samples support such distortions (and/or heterogeneous Fe occupancy by Mo) which are well-known to be encountered in high pressure samples with transition metals[74] in octahedral symmetries.[73] Bond valence sum analyses confirmed that Mo can exist in six-coordinated geometries with the bond distances modeled for the coprecipitated post-transformed samples.

There are several factors that could contribute to local distortions of the polyhedra. These include the following: fast dehydration and rearrangement of ferrihydrite, high temperature (up to 200 °C) and pressure (not measured) of the reactions, differences in Fe (0.64 Å) and Mo (0.59 Å) ionic radii, and different degrees of Mo substitution within the hematite structure. In addition, the initial transformation pH (i.e., 7 and 8.5) does not appear to influence the Mo speciation in the end product (Figure 4).

V-XAS. The V K-edge XANES spectra for V adsorbed onto and coprecipitated with ferrihydrite are similar to the Na_3VO_4 standard spectra and feature a pre-edge peak at about 5469.5 eV and a shoulder at 5474.9 eV (Figure 4A,B). Comparison of the V K-edge XANES of the standard with the adsorbed and coprecipitated samples suggests that V is present as V(V) and is tetrahedrally coordinated.[75]

The lower intensity (ca. 60%) of the pre-edge peak at 5470 eV of V K-edge XANES of the transformed coprecipitated samples compared with that of the pretransformed samples or the Na_3VO_4 standard (but also higher than in V K-edge XANES spectrum of a V(III) species, i.e., V_2O_3, and V(IV) species such as V_4O_7[75]) indicates a change in the structural geometry of V in the hematite structure, possibly due to
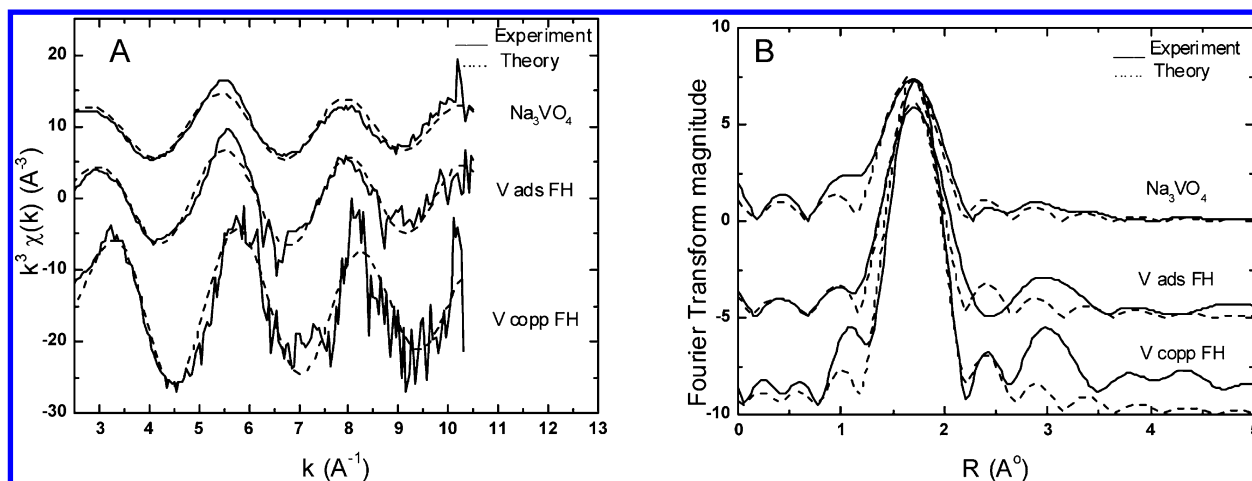
Figure 5. Summary of k^3 weighted (A) V-EXAFS spectra and (B) calculated Fourier transforms for EXAFS spectra for coprecipitated and adsorbed samples and Na_3VO_4 standard.

Table 3. Summary of V EXAFS Data Fits and Appropriate Standards

sample	bond type	coordination number	interatomic distance, R (Å)	σ^2-factor[b]	R-factor[c]
Na_3VO_4	V—O	4	1.70 ± 0.02	0.003 ± 0.004	0.01
$Na_3VO_4 \cdot 3H_2O$[a]	V—O	3	1.72		
	V—O	1	1.70		
V ads FH, pH7	V—O	4	1.70 ± 0.02	0.002 ± 0.004	0.02
V copp FH, pH7	V—O	4	1.68 ± 0.02	0.004 ± 0.003	0.009

[a]$Na_3VO_4 \cdot 3H_2O$ structure (ICSD 62533) after Kato and Takayama-Muromachi.[79] [b]σ^2 is the mean-square disorder in the distribution of interatomic distances.[56] [c]R-factor is the sum of the residual: a measure of the percentage misfit between the data and theory.[56]

octahedral coordination. In a comparison of our XANES spectra with XANES profiles of relevant V oxide compounds studied by Wong et al.,[75] it can be seen that the position of the pre-edge peak in the transformed sample spectrum (5468.6 eV) is quite similar to the pre-edge features of V_2O_4 (IV) (5469.7 eV using our calibration value for V foil of 5464.3 eV). This indicates that V could have been at least partially reduced to V(IV) during the transformation reaction, possibly due limited O_2 concentration in the transformation chamber.

The EXAFS of V adsorbed onto and coprecipitated with ferrihydrite and the standard Na_3VO_4 showed similar features (Figure 5). The best fitting parameters give V—O bond distances of 1.68 and 1.70 Å, which are typical of a tetrahedrally coordinated vanadate species. The V—O distance found in tetrahedral VO_4 varies between 1.65 and 1.76 Å, as a function of the neighboring metals in each specific compounds and their structural geometry [i.e., $MnNa(VO_4)$,[76] $NaCaVO_4$,[77] $Cd_4Na-(VO_4)_3$[78]]. These EXAFS fitting results indicate that V is adsorbed and coprecipitated as vanadate onto the surface of ferrihydrite and within the ferrihydrite structure (Table 3).

Differences in amplitudes of the k^3-weighted EXAFS and in the intensity of the first peak in Fourier transform between the Na_3VO_4 standard and the adsorbed and coprecipitated samples possibly indicate different degrees of hydration or various scattering effects from the neighboring atoms in the V tetrahedral structure. The Fourier transform of the V adsorbed ferrihydrite EXAFS displays a broad peak at 2.97 Å, and that of the coprecipitated ferrihydrite displays a second peak at 2.40 Å and a third broad peak at a distance of 2.98 Å. No sensible model could be built that fitted these peaks successfully. However, these peaks might result from various V—Fe

scattering paths from possible inner sphere surface complexes on ferrihydrite.[2,9]

Modeling V in the Fe site in hematite did not refine to a sensible set of parameters or a good fit. Thus, we can only conclude that V XANES, as V EXAFS, tells us little about the incorporation mode of V in the hematite structure, other than that there are probably a mixture of different sites, some of which are octahedral (see the data in Figure SI 7).

Transformation Kinetics: Energy Dispersive X-ray Diffraction. *i. Pure Ferrihydrite Transformation at pH 8 and Ionic Strength 0.7.* The growth of the hematite (110) and goethite (110) diffraction peaks at all temperatures as a function of time is shown in Figure 6 and Figure SI 2. In all the on-line, *in situ* transformation experiments carried out at temperatures >140 °C, the diffraction patterns showed that hematite is the main transformation end product. The EDXRD data collected from the experiment run at temperatures 140 °C revealed that minor amounts of goethite were present during the transformation (Figure SI 2). Differently, goethite was observed as an intermediate (minor amount) in the off-line *ex situ* experiments at 160 °C (Figure SI 1). This is likely due to the EDXRD spectra being collected from solids suspended in solution, though this is one of the advantages of the EDXRD technique: it leads to a high background in the *in situ* EDXRD spectra.[57] The high background may have masked minor phases (i.e., goethite).

The EDXRD data revealed that the degree of ferrihydrite transformation to hematite is temperature dependent (Figures 6 and 7A,B). The induction time, for the appearance of hematite, decreases with increasing temperature, whereas the rate of crystallization increases with increasing temperature (Table 4). Specifically, in the pure ferrihydrite system at 240
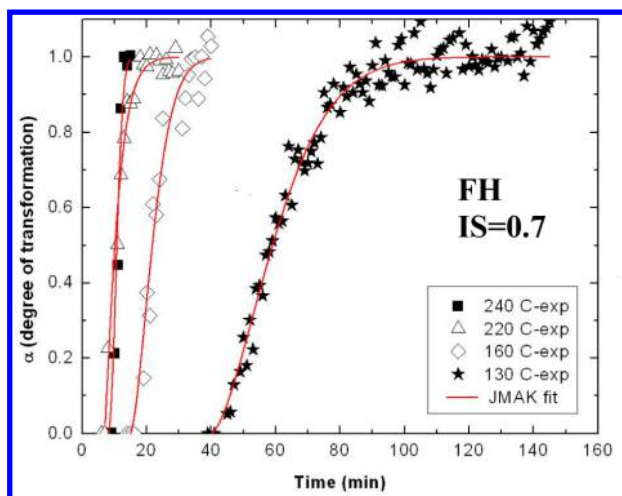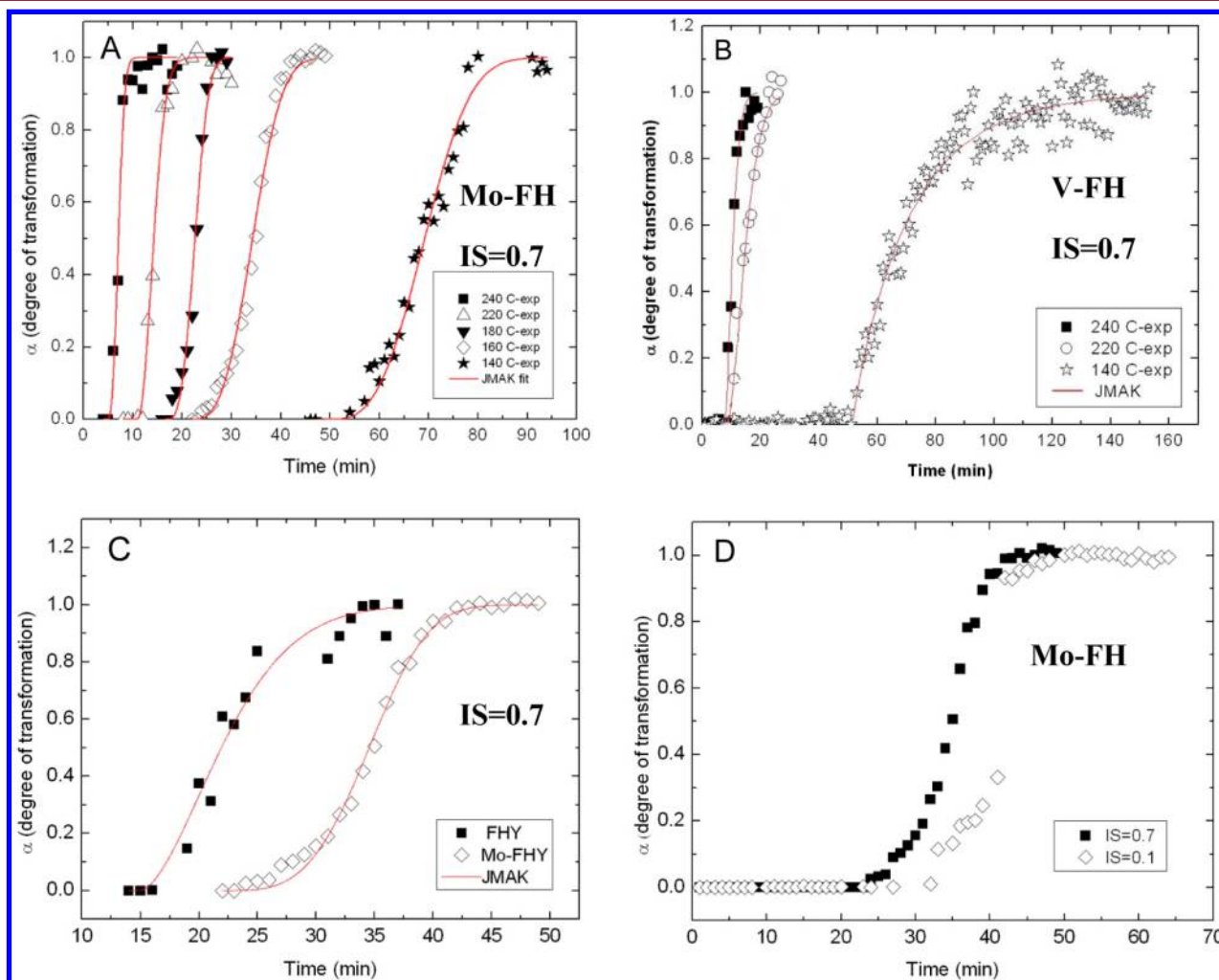
Figure 6. Degree of transformation of pure ferrihydrite to hematite as a function of temperature in the *in situ* EDXRD experiments.

°C, the (110) peak of hematite was first observed after 8 min, and the reaction was complete after 15 min, while at lower temperature (130 °C) hematite started to form only after 40

min, and the reaction was complete only after ~100 min (Figure 6).

ii. Effect of Coprecipitated Mo and V on the Ferrihydrite. The analyses of supernatant from the Mo and V coprecipitated ferrihydrite experiments revealed that the starting materials used in the *in situ* transformation experiments contain ~3.1 mg Mo g^{-1} and 1.6 mg V g^{-1} (or ~0.03 mM Mo/V g^{-1}). The EDXRD results showed that the presence of Mo and V (in coprecipitated ferrihydrite, Figure 7A,B) increased the induction time of the transformations, compared to pure FH system (Figure 6) at the same ionic strength (0.7) and temperature (160 °C as example). This effect could be observed clearly at low temperature (i.e., 140 °C) at which the induction time increased by up to 32% and 38% in the Mo-FH and V-FH systems, respectively (Figure 7C,B, and Table 4). However, at higher temperatures (above 220 °C), this increase was not observed, possibly because the reaction was too rapid or the influence of temperature outweighed the influence of the metals.

Comparison of the reaction rates in the Mo system at high (0.7) and low (0.1) ionic strengths (Figure 7D) revealed that lowering the ionic strength retards the ferrihydrite transformation to hematite. For example, at 160 °C and higher ionic

Figure 7. Degree of transformation of ferrihydrite to hematite as a function of time, temperature, and ionic strength for (A) Mo-FH at IS = 0.7; (B) V-FH at IS = 0.7; (C) pure FH and Mo-FH at 160 °C and IS = 0.7; (D) Mo-FH at 160 °C and IS = 0.7 and IS = 0.1. Symbols are experimental data points, and lines represent the JMAK fits.

Table 4. JMAK Fitting Parameters (with t_o Fixed As Given by the Experimental Data) and Activation Energies for Hematite Formation with and without Mo and V for the Experiments at IS = 0.7

	Mo-FH					V-FH					FH			
T (°C)	$k \times 10^4$ (s^{-1})	t_o (s)	m	R^2	T (°C)	$k \times 10^4$ (s^{-1})	t_o (s)	m	R^2	T (°C)	$k \times 10^4$ (s^{-1})	t_o (s)	m	R^2
240	55 ± 8	267 ± 23	3	0.980	240	41.3 ± 3.3	422.5 ± 17.5	2	0.993	240	62 ± 6	519 ± 12	2	0.981
220	30 ± 2	574 ± 24	3	0.987	220	19 ± 1	445.5 ± 25.2	2	0.992	220	26 ± 1	319 ± 24	2	0.985
180	27 ± 0.2	1032 ± 21	3	0.988	140	4.5 ± 0.2	2213.5 ± 77.9	2	0.980	160	19 ± 3	887 ± 58	2	0.965
160	13 ± 0.5	1408 ± 26	3	0.994						140	n.d.	1900^a	n.d	
140	6.8 ± 0.3	2845 ± 66	3	0.980						130	5.8 ± 0.2	2144 ± 58	2	0.976

	Mo-FH	V-FH	FH
$E_{a,cryst.AA}$ (kJ/mol)	33 (±6)	36 (±7)	31 (±8)
$E_{a,cryst.TGF}^{b}$ (kJ mol^{-1})	39 (±3)	26 (±10)	26 (±5)

^{a}Only the beginning of the transformation was recorded for this experiment. $^b E_{a,cryst.TGF}$ is the apparent activation energy of crystallization derived using "time to a given fraction" method for t = 50%.[67] ^{c}Fixed values.

strength the induction time of the transformation was reduced from 32 to 23 min (i.e., about 30%, Figure 7D).

Fitting the degree of the transformation of ferrihydrite versus time with the JMAK model yielded values (Table 4) for rate constant (k), induction time (t_o), and exponential factor (m). The results showed that, in all three systems studied, the hematite crystallization rate increases with temperature, while the induction times decreases with increasing temperature.

The m values obtained from the JMAK fits (Table 4) ranged between 2 and 3. The classification by Hulbert[63] for m values indicate that values of 2−3 are suggestive of 2D phase boundary controlled growth. Thus, our values supports the two-dimensional growth of the hematite plates.

Using the Arrhenius approach the apparent activation energies of crystallization for hematite for all systems were derived but show that Mo and V (at all concentrations) did not have any significant effect on the crystallization activation energy (Table 4), relative to pure ferrihydrite system. Shaw et al.[33] calculated, via the Arrhenius approach, an activation energy for hematite crystallization at pH 10.7 of 69 ($\pm$6) kJ mol^{-1}. This higher value for hematite formation under alkaline conditions compared with the values obtained in the present study (38 $\pm$ 8; Table 4) can be explained by the difference in pH, i.e., alkaline versus near neutral conditions, 2.7 pH unit difference.[11,32,33,42,80,81]

The apparent activation energies of crystallization to hematite ($E_{a,cryst.TGF}$, Table 4) calculated using the "time to a given fraction" (TGF) approach[67] resulted in values comparable to those obtained from the Arrhenius approach. Thus, using this approach we recalculated the crystallization activation energy of goethite (without phosphate) from Shaw et al.,[33] using the "time to a given fraction" approach,[67] and obtained a very good agreement (67 $\pm$ 4 kJ mol^{-1}) with the activation energy calculated via the Arrhenius approach, again indicating that this approach can be applied to extrapolate and calculate activation energies for mineral crystallizations at different temperatures.

Using the dependence of rate constant and the induction time on temperature (i.e., the Arrhenius plots obtained in the *in situ* experiments, Figures SI 3 and SI 4), extrapolations can be used to calculate the time frame for ferrihydrite transformation (and metal sequestration) at low temperatures. This approach can be used to calculate time frames for metal sequestration by iron (oxyhydr)oxides in soils, sediments, and marine systems (i.e., mid-ocean ridge hydrothermal systems).

Summary, Implications, and Conclusions. Quantitative results of Mo and V uptake by ferrihydrite and their fate after its transformation to hematite showed that more than 90% of Mo and 94% of V were sequestered in the hematite structure after adsorption to ferrihydrite, while 94% of Mo and 100% of V were immobilized after coprecipitation with ferrihydrite.

The Mo and V present in the adsorbed and coprecipitated samples are initially taken up by ferrihydrite as tetrahedrally coordinated molybdate and vanadate, respectively. After the ferrihydrite was transformed to hematite V becomes partially reduced to V(IV). Mo became incorporated in the hematite structure at mainly distorted octahedral sites. These distortions may be due to the high temperature and pressure used in the transformation experiments as well as the fast dehydration rearrangement during the crystallization of hematite from ferrihydrite.

The results from the current study show that at near neutral pH hematite is the main transformation end product and that

the crystallization is temperature dependent. At high temperatures (i.e., 200 °C) hematite is the sole transformation end product whereas, at lower temperatures, goethite is a minor product.

The *in situ* and time-resolved EDXRD data showed that ferrihydrite transformation to hematite occurred via 2D phase boundary growth of hematite plates following a dehydration, rearrangement mechanism. High temperature and higher ionic strength primarily affected the crystallization process. The presence of Mo and V had no significant effect on the crystallization rate as well as the activation energies. Our kinetic results can help quantify the time scales of Mo and V sequestration in various environments where ferrihydrite forms.

We also reported the first rate constants, induction times, and activation energies for three different systems (pure FH, V-FH, Mo-FH) at near neutral pH conditions. These are important for a plethora of natural systems (i.e., seawater hydrothermal systems, soil and wastewater remediation processes, etc.) where scavenging processes play a significant role in the Mo and V cycles. For example, our data can help estimate the impact of hydrothermal systems on the Mo and V budget to global ocean. This could be done by using specific ocean circulation models and assuming that the whole ocean reservoir is passing through the hydrothermal systems once every 10^3–10^4 years[82,83] and Mo and V concentration in the water column is 10 mg L^{-1}[84] and 2–3 μg L^{-1},[85] respectively. As example, Trefry and Metz, estimated that 10–16% of the riverine V inputs are removed from seawater by scavenging processes through iron oxides originating from hydrothermal vents.[17]

ASSOCIATED CONTENT

ⓢ Supporting Information

The Supporting Information is available free of charge on the ACS Publications website at DOI: 10.1021/acs.cgd.5b00173.

> Figures including XRD analyses, experimental progression plots, EXAFS spectra, and XANES spectra (PDF)

AUTHOR INFORMATION

Corresponding Authors
*Phone: +40(0) 755356866. E-mail: b_loredana@yahoo.com.
*Phone: +49 (0)331 288 28 970. E-mail: benning@gfz-potsdam.de.

Notes
The authors declare no competing financial interest.

ACKNOWLEDGMENTS

REFERENCES

(1) Cornell, R. M.; Schwertmann, U. *The Iron Oxides: Structure, Proprieties, Reactions, Occurances and Uses*; Wiley-VCH GmbH&KGaA: Weinheim, 2003.

(2) Peacock, C. L.; Sherman, D. M. Vanadium (V) Adsorption onto Goethite (α-FeOOH) at pH 1.5 to 12: a surface complexation model based on ab initio molecular geometries and EXAFS spectroscopy. *Geochim. Cosmochim. Acta* **2004**, *68*, 1723−1733.

(3) Rout, K.; Mohapatra, M.; Anand, S. 2-Line Ferrihydrite: Synthesis, Characterization and its Adsorption Behaviour for Removal of Pb(II), Cd(II), Cu(II) and Zn(II) from Aqueous Solutions. *Dalton Trans.* **2012**, *41*, 3302−3312.

(4) Martínez, C. E.; McBride, M. B. Solubility of Cd2+, Cu2+, Pb2+, and Zn2+ in Aged Coprecipitates with Amorphous Iron Hydroxides. *Environ. Sci. Technol.* **1998**, *32*, 743−748.

(5) Martínez, C. E.; McBride, M. B. Cd, Cu, Pb, and Zn Coprecipitates in Fe Oxide Formed at Different pH: Aging Effects on Metal Solubility and Extractability by Citrate. *Environ. Toxicol. Chem.* **2001**, *20*, 122−126.

(6) Hochella, M. F.; Kasama, T.; Putnis, A.; Putnis, C. V.; Moore, J. N. Environmentally Important, Poorly Crystalline Fe/Mn Hydrous Oxides: Ferrihydrite and a Possibly New Vernadite-like Mineral from the Clark Fork River Superfund Complex. *Am. Mineral.* **2005**, *90*, 718−724.

(7) Rhoton, F.; Bigham, J. Phosphate Adsorption by Ferrihydrite-Amended Soils. *J. Environ. Qual.* **2005**, *34*, 890−896.

(8) Vu, H. P.; Shaw, S.; Brinza, L.; Benning, L. G. Partitioning of Pb(II) During Goethite and Hematite Crystallization: Implications for Pb Transport in Natural Systems. *Appl. Geochem.* **2013**, *39*, 119−128.

(9) Sherman, D. M.; Randall, S. R. Surface Complexation of Arsenic (V) to Iron (III) (Hydr)oxides: Structural Mechanism from Ab Initio Molecular Geometries and EXAFS Spectroscopy. *Geochim. Cosmochim. Acta* **2003**, *67*, 4223−4230.

(10) Vu, H. P.; Moreau, J. W. Thiocyanate Adsorption on Ferrihydrite and its Fate During Ferrihydrite Transformation to Hematite and Goethite. *Chemosphere* **2015**, *119*, 987−993.

(11) Vu, H. P.; Shaw, S.; Brinza, L.; Benning, L. G. Crystallization of Hematite (alpha-Fe$_2$O$_3$) under Alkaline Condition: The Effects of Pb. *Cryst. Growth Des.* **2010**, *10*, 1544−1551.

(12) Neaman, A.; Martínez, C. E.; Trolard, F.; Bourrié, G. Trace Element Associations with Fe- and Mn-oxides in Soil Nodules: Comparison of Selective Dissolution with Electron Probe Microanalysis. *Appl. Geochem.* **2008**, *23*, 778−782.

(13) Feely, R. A.; Massoth, G. J.; Baker, E. T.; Lebon, G. T.; Geiselman, T. L. Tracking the Dispersal of Hydrothermal Plumes from the Juan de Fuca Ridge Using Suspended Matter Compositions. *J. Geophys. Res.* **1992**, *97*, 3457−3468.

(14) Raiswell, R.; Canfield, D. E. The Iron Biogeochemical Cycle Past and Present. *Geochemical Perspectives* **2012**, *1*, 1−220.

(15) Feely, R. A.; Massoth, G. J.; Baker, E. T.; Cowen, J. P.; Lamb, M. F.; Krogslund, K. A. The Effect of Hydrothermal Processes on Midwater Phosphorus Distributions in the Northeast Pacific. *Earth Planet. Sci. Lett.* **1990**, *96*, 305−318.

(16) Metz, S.; Trefry, J. H. Scavenging of Vanadium by Iron Oxides in Hydrotermal Plumes. *Eos* **1988**, *69*, 1480.

(17) Trefry, J. H.; Metz, S. Role of Hydrothermal Precipitates in the Geochemical Cycling of Vanadium. *Nature* **1989**, *342*, 531−533.

(18) Rancourt, D. G.; Fortin, D.; Pichler, T.; Thibault, P.-J.; Lamarche, G.; Morris, R. V.; Mercier, P. H. J. Mineralogy of a Natural As-rich Hydrous Ferric Oxide Coprecipitate Formed by Mixing of Hydrothermal Fluid and Seawater: Implications Regarding Surface Complexation and Color Banding in Ferrihydrite Deposits. *Am. Mineral.* **2001**, *86*, 834−851.

(19) Kashiwabara, T.; Takahashi, Y.; Tanimizu, M. XAFS Study on the Mechanism of Isotopic Fractionation of Molybdenum During its Adsorption on Ferromanganese Oxides. *Geochem. J.* **2009**, *43*, e31−e36.

(20) Kashiwabara, T.; Takahashi, Y.; Tanimizu, M.; Usui, A. Molecular-scale Mechanisms of Distribution and Isotopic Fractionation of Molybdenum Between Seawater and Ferromanganese Oxides. *Geochim. Cosmochim. Acta* **2011**, *75*, 5762−5784.

(21) Edmond, J. M.; Measures, C.; McDuff, R. E.; Chan, L. H.; Collier, R.; Grant, B.; Gordon, L. I.; Corliss, J. B. Ridge Crest

Hydrothermal Activity and the Balances of the Major and Minor Elements in the Ocean: The Galapagos data. *Earth Planet. Sci. Lett.* **1979**, *46*, 1−18.

(22) German, C. R.; Bourles, D. L.; Brown, E. T.; Hergt, J.; Colley, S.; Higgs, N. C.; Ludford, E. M.; Nelsen, T. A.; Feely, R. A.; Raisbeck, G.; Yiou, F. Hydrothermal Scavenging on the Juan de Fuca Ridge: Evidence from ridge-flank sediments. *Geochim. Cosmochim. Acta* **1997**, *61*, 4067−4078.

(23) Hille, R. The Mononuclear Molybdenum Enzymes. *Chem. Rev.* **1996**, *96*, 2757−2816.

(24) Mendel, R. R. Molybdenum: biological activity and metabolism. *Dalton Trans.* **2005**, *7*, 3404−3409.

(25) Burgess, B. K.; Lowe, D. J. Mechanism of Molybdenum Nitrogenase. *Chem. Rev.* **1996**, *96*, 2983−3012.

(26) Levinton, J. S. *Marine Biology: Function, Biodiversity, Ecology*; Oxford University Press: Oxford, U.K., 2010.

(27) Das, A. K.; Chakraborty, R.; Cervera, M. L.; de la Guardia, M. A review on molybdenum determination in solid geological samples. *Talanta* **2007**, *71*, 987−1000.

(28) Venkataraman, B. V.; Sudha, S. Vanadium Toxicity. *Asian J. Exp. Sci.* **2005**, *19*, 127−134.

(29) Nriagu, J. O. *Vanadium in the Environment, Part 2, Health Effects*; John Wiley and Sons: New York, 1998.

(30) Siebert, C.; Nagler, T. F.; von Blanckenburg, F.; Kramers, J. D. Molybdenum Isotope Records as a Potential New Proxy for Paleoceanography. *Earth Planet. Sci. Lett.* **2003**, *211*, 159−171.

(31) Feely, R. A.; Trefry, J. H.; Lebon, G. T.; German, C. R. The Relationship Between P/Fe and V/Fe Ratios in Hydrothermal Precipitaes and Dissolved Phosphate in Seawater. *Geophys. Res. Lett.* **1998**, *25*, 2253−2256.

(32) Schwertmann, U.; Murad, E. Effect of pH on Formation of Goethite and Hematite from Ferrihydrite. *Clays Clay Miner.* **1983**, *31*, 277−284.

(33) Shaw, S.; Pepper, S. E.; Bryan, N. D.; Livens, F. R. The Kinetics and Mechanisms of Goethite and Hematite Crystallization Under Alkaline Conditions, and in the Presence of Phosphate. *Am. Mineral.* **2005**, *90*, 1852−1860.

(34) Galvez, N.; Barron, V.; Torrent, J. Effect of Phosphate on the Crystallization of Hematite, Goethite, and Lepidocrocite from Ferrihydrite. *Clays Clay Miner.* **1999**, *47*, 304−311.

(35) Lin, X.; Burns, R. C.; Lawrance, G. A. Effect of Cadmium (II) and Anion Type on the Ageing of Ferrihydrite and its Subsequent Leaching Under Neutral and Alkaline Conditions. *Water, Air, Soil Pollut.* **2003**, *143*, 155−177.

(36) Yee, N.; Shaw, S.; Benning, L. G.; Nguyen, T. H. The Rate of Ferrihydrite Transformation to Goethite via the Fe(II) Pathway. *Am. Mineral.* **2006**, *91*, 92−96.

(37) Cudennec, Y.; Lecerf, A. The Transformation of Ferrihydrite into Goethite or Hematite, Revisited. *J. Solid State Chem.* **2006**, *179*, 716−722.

(38) Das, S.; Hendry, M. J.; Essilfie-Dughan, J. Transformation of Two-line Ferrihydrite to Goethite and Hematite as a Function of pH and Temperature. *Environ. Sci. Technol.* **2011**, *45*, 268−275.

(39) Hamzaoui, A.; Mgaidi, A.; Megriche, A.; El Maaoui, M. Kinetic Study of Goethite Formation from Ferrihydrite in Alkaline Medium. *Ind. Eng. Chem. Res.* **2002**, *41*, 5226−5231.

(40) Schwertmann, U.; Friedl, J.; Stanjek, H. From Fe(III) Ions to Ferrihydrite and then to Hematite. *J. Colloid Interface Sci.* **1999**, *209*, 215−223.

(41) Jolivet, J.-P.; Chaneac, C.; Tronc, E. Iron Oxide Chemistry. From Molecular Clustters to Extended Solid Networks. *Chem. Commun.* **2004**, *5*, 481−487.

(42) Davidson, L. E.; Shaw, S.; Benning, L. G. The Kinetics and Mechanisms of Schwertmannite Transformation to Goethite and Hematite Under 2 Alkaline Conditions. *Am. Mineral.* **2008**, *93*, 1326−1337.

(43) Vu, H. P.; Shaw, S.; Brinza, L.; Benning, L. G. Crystallization of Hematite (a-Fe2O3) Under Alkaline Condition: the Effects of Pb. *Cryst. Growth Des.* **2010**, *10*, 1544−1551.

(44) Willey, J. D. The Effect of Ionic Strength on the Solubility of an Electrolyte. *J. Chem. Educ.* **2004**, *81*, 1644.

(45) Burrows, N. D.; Hale, C. R. H.; Penn, R. L. Effect of Ionic Strength on the Kinetics of Crystal Growth by Oriented Aggregation. *Cryst. Growth Des.* **2012**, *12*, 4787−4797.

(46) Cappellen, V. L. K. V. *The Effects of Ionic Strength and Aggregation on Crystal Growth Kinetics: An Application of Photon Correlation Spectroscopy*; School of Civil and Environmental Engineering, Georgia Institute of Technology: Atlanta, GA, 1996. Directed by Christine L. Tiller, 1995.

(47) Tai, C. Y.; Hsu, H.-P. Crystal Growth Kinetics of Calcite and its Comparison with Readily Soluble Salts. *Powder Technol.* **2001**, *121*, 60−67.

(48) Brinza, L.; Benning, L. G.; Statham, P. J. Adsorption Studies of Mo and V onto Ferrihydrite. *Mineral. Mag.* **2008**, *72*, 385−388.

(49) Brinza, L. *Interactions of Molybdenum and Vanadium with Iron Nanoparticles*. Ph.D. Thesis, University of Leeds, Leeds, U.K., June 2010.

(50) Zhao, J.; Feng, Z.; Huggins, F. E.; Shah, N.; Huffman, G. P.; Wender, I. Role of Molybdenum at the Iron Oxides Surface. *J. Catal.* **1994**, *148*, 194−197.

(51) Cornell, R. M.; Schwertmann, U. *The Oxides in the Laboratory*; Wiley-VCH: Weinheim, 2000.

(52) Viollier, E.; Inglett, P. W.; Hunter, K.; Roychoudhury, A. N.; Cappellen, P. V. The Ferrozine Method Revisited: Fe(II)/Fe(III) Determination in Natural Waters. *Appl. Geochem.* **2000**, *15*, 785−790.

(53) Carvalho, F. M. S.; Abrao, A. Sorption and Desorption of Molybdenum in Alumina Microspheres. *J. Radioanal. Nucl. Chem.* **1997**, *218*, 259−262.

(54) Bilsborrow, R.; Atkinson, P.; Bliss, N.; Dent, A.; Dobson, B.; Stephenson, P.; Wide-aperture, A. Dynamically Focusing Sagittal Monochromator for X-ray Spectroscopy and Diffraction. *J. Synchrotron Radiat.* **2006**, *13*, 54−58.

(55) Mosselmans, F.; Cavill, S.; Peach, A.; Keylock, S.; Gregory, S.; Quinn, P.; Rosell, J. R.; Atkinson, K.; Dent, A.; Diaz-Moreno, S.; Leicester, P. I18-the Microfocus Spectroscopy Beamline at the Diamond Light Source. *J. Synchrotron Radiat.* **2009**, *16*, 818−824.

(56) Ravel, B.; Newville, M. A. ATHENA, ARTEMIS, HEPHAESTUS: Data Analysis for X-ray Absorption Spectroscopy Using IFEFFIT. *J. Synchrotron Radiat.* **2005**, *12*, 537−541.

(57) Parise, J. B. Synchrotron Studies of Phase Transformations. In *Transformation Processes in Minerals*; Redfern, A. T. S., Carpenter, A. M., Eds.; Reviews in Mineralogy and Geochemistry; Mineralogical Society of America: Cambridge, U.K., July 2000; Vol. 39, p 318.

(58) Cheary, R. W.; Coelho, A. A. *Programs XFIT and FOURYA Deposited in CCP14 Powder Diffraction Library*; Engineering and Physical Sciences Research Council, Daresbury Laboratory: Warrington, U.K., 1996.

(59) Murray, J.; Kirwan, L.; Loan, M.; Hodnett, B. K. In-situ Synchrotron Diffraction Study of the Hydrothermal Transformation of Goethite to Hematite in Sodium Aluminate Solutions. *Hydrometallurgy* **2009**, *95*, 239−246.

(60) Avrami, M. Granulation, Phase Change, and Microstructure Kinetics of Phase Change. III. *J. Chem. Phys.* **1941**, *9*, 177.

(61) Avrami, M. Kinetics of phase change. I General Theory. *J. Chem. Phys.* **1939**, *7*, 1103−1112.

(62) Avrami, M. Kinetics of Phase Change. II Transformation-Time Relations for Random Distribution of Nuclei. *J. Chem. Phys.* **1940**, *8*, 212−224.

(63) Hulbert, S. F. Models of Solid-State Reactions in Powder Compacts: A review. *J. Br. Ceram. Soc.* **1969**, *6*, 11−20.

(64) *Origin Pro 8*; OriginLab: Northampton, MA, 2007.

(65) Finney, E. E.; Finke, R. G. Nanocluster Nucleation and Growth Kinetic and Mechanistic Studies: A Review Emphasizing Transition-metal Nanoclusters. *J. Colloid Interface Sci.* **2008**, *317*, 351−374.

(66) Khawam, A.; Flanagan, D. R. Solid-State Kinetic Models: Basics and Mathematical Fundamentals. *J. Phys. Chem. B* **2006**, *110*, 17315−17328.

(67) Putnis, A. *Introduction to Mineral Sciences*; Cambridge University Press: Cambridge, U.K., 1992; p 457.

(68) Janney, D. E.; Cowley, J. M.; Buseck, P. R. Transmission Electron Microscopy of Synthetic 2- and 6-Line Ferrihydrite. *Clays Clay Miner.* **2000**, *48*, 111−119.

(69) Essilfie-Dughan, J.; Pickering, I. J.; Hendry, M. J.; George, G. N.; Kotzer, T. Molybdenum Speciation in Uranium Mine Tailings using X-ray Absorption Spectroscopy. *Environ. Sci. Technol.* **2011**, *45*, 455−60.

(70) Matsumoto, K.; Kobayashi, A.; Sasaki, Y. The Crystal Structure of Sodium Molybdate Dihydrate, Na$_2$MoO$_4$·2H$_2$O. *Bull. Chem. Soc. Jpn.* **1975**, *48*, 1009−1013.

(71) Wolska, E.; Schwertmann, U. Nonstoichiometric Structures During Dehydroxylation of Goethite. *Z. Kristallogr.* **1989**, *189*, 223−237.

(72) Radhakrishnan, R.; Reed, C.; Oyama, S. T.; et al. Variability in the Structure of Supported MoO3 Catalysts: Studies Using Raman and X-ray Absorption Spectroscopy with ab Initio Calculations. *J. Phys. Chem., B* **2001**, *105*, 8519−8530.

(73) Halcrow, M. A. Jahn-Teller Distortions in Transition Metal Compounds, and Their Importance in Functional Molecular and Inorganic Materials. *Chem. Soc. Rev.* **2013**, *42*, 1784−1795.

(74) Brown, D. *The Chemical Bond in Inorganic Chemistry: The Bond Valence Model*; Oxford University Press: Oxford, U.K., 2006.

(75) Wong, J.; Lytle, F. W.; Messmer, R. P.; Maylotte, D. H. K-edge Absorption Spectra of Selected Vanadium Compounds. *Phys. Rev. B: Condens. Matter Mater. Phys.* **1984**, *30*, 5596−5610.

(76) Yahia, H. B.; Gaudin, E.; Boulahya, K.; Darriet, J.; Sun, W.-J.; Whangbo, M.-H. Synthesis and Characterization of the Crystal Structure and Magnetic Properties of the Ternary Manganese Vanadate Na Mn V O4. *Inorg. Chem.* **2010**, *49*, 8578−8582.

(77) Ijdo, D. J. W. Calcium Sodium Vanadate at 300 K: Structure Refinement by Powder Neutron Diffraction. *Acta Crystallogr., Sect. B: Struct. Crystallogr. Cryst. Chem.* **1982**, *38*, 923−925.

(78) Amara, M. B.; Vlasse, M.; Olazcuaga, R.; Flem, G. L. The Structure of Cadmium Sodium Orthovanadate Cd4Na(VO4)3. *Acta Crystallogr., Sect. B: Struct. Crystallogr. Cryst. Chem.* **1979**, *35*, 50−52.

(79) Kato, K.; Takayama-Muromachi, E. Die Struktur des Trinatriumvanadattrihydrats. *Acta Crystallogr., Sect. C: Cryst. Struct. Commun.* **1987**, *43*, 1030.

(80) Fischer, W. R.; Schwertmann, U. Formation of Hematite from Amorphous Iron (III) hydroxide. *Clays Clay Miner.* **1975**, *23*, 33−37.

(81) Schwertmann, U.; Stanjek, H.; Becher, H. H. Long-term In Vitro Transformation of 2-line Ferrihydrite to Goethite/Hematite at 4, 10, 15 and 25 Degrees C. *Clay Miner.* **2004**, *39*, 433−438.

(82) Statham, P. J.; German, C. R.; Connelly, D. P. Iron (II) Distribution and Oxidation Kinetics in Hydrothermal Plumes at the Kairei and Edmond Vent Sites, Indian Ocean. *Earth Planet. Sci. Lett.* **2005**, *236*, 588−596.

(83) Tuner, D. R.; Hunter, K. A. *The Biogeochemistry of Iron in Seawater*; John Wiley & Son Ltd.: London, 2001.

(84) Chester, R. *Marine Geochemistry*; Unwin Hyman Ltd.: London, 1990.

(85) Ferreira, S. L. C.; Queiroz, A. S.; Fernandes, M. S.; dos Santos, H. C. Application of Factorial Designs and Doehlert Matrix in Optimization of Experimental Variables Associated with the Preconcentration and Determination of Vanadium and Copper in Seawater by Inductively Coupled Plasma Optical Emission Spectrometry. *Spectrochim. Acta, Part B* **2002**, *57*, 1939−1950.